Journal Article

Design, Simulation and Measurement of Metapocket: An All-textile Reflective Metasurface for On-Body Smartphone Radiation Improvement

Zhai, M., Tian, W., Pei, R., Xu, C., Leach, M., Lim, E. G., Wang, Z., Wang, J., Hua, Q., Akinsolu, M. O., Liu, B., and Huang, Y

Design, Simulation and Measurement of Metapocket: An All-textile Reflective Metasurface for On-body Smartphone Radiation Improvement

Menglin Zhai, Wandai Tian, Rui Pei, Chen Xu, Mark Leach, Eng Gee Lim, *senior member*, *IEEE*, Zhao Wang, Jingchen Wang, Qiang Hua, Mobayode Akinsolu, Bo Liu, *senior member*, *IEEE*, and Yi Huang, *fellow*, *IEEE*

***Abstract*—A polarization-independent all-textile reflective metasurface – the metapocket, is presented in this paper. This design aims at enhancing gain, and radiation efficiency and reducing the Specific Absorption Rate (SAR) of a smartphone antenna when it is placed inside a jacket pocket close to the human body. During the design process, the state-of-the-art smartphone structure, the impact of varying unit cell numbers on reflectivity and the nature of textile materials have been taken into consideration. Also, an AI-driven antenna design algorithm is employed. Full wave simulations with a voxel human body model and real measurement with smartphone vivo iQOO validate the effectiveness of the metapocket. The effect of applying the metapocket is quantified with an anechoic chamber radiation pattern measurement and a reverberation chamber radiation efficiency measurement. Results reveal a 3.17 dB realized gain increase, 34.37% radiation efficiency improvement, and a more than 85% SAR reduction are achieved in the on-body scenario. The proposed design has a high potential for improving smartphone communication with various Internet of Things (IoT) and wearable devices.**

***Index Terms*—Metapocket; Radiation Efficiency; Reverberation Chamber Measurement; Metasurface; Smartphone antenna; Textile materials.**

I. INTRODUCTION

WITH the rapid development of wireless communication technology, smartphones have become an indispensable part of people's daily lives, serving functions such as communication and entertainment [1]. State-of-the-art smartphones have been equipped with high-performance processor chips and an ever-going amount of memories. Meanwhile, with the increasing number of wearable electronics and IoT devices such as smart watches, smart gloves, smart healthcare, etc [2], [3], the requirements for interactive wireless communication hence on the radio frequency links are getting higher [4], [5]. As a key processing node in wireless communication, communication performance of smartphones can be significantly improved by optimizing the antenna performance [6], [7].

Fig. 1 shows a scenario centered with a smartphone on the human body, including various wearable electronics and hence providing services like health care, localization, edge computing cloud connectivity, etc. As the most computationally powerful device in this scenario, a solid commutation link between the smartphone and other devices becomes crucial. The presence of the human body would have impacts on the radiation from the smartphone antenna, especially at the commonly-used 2.45 GHz frequency band due to its relatively larger wavelength and absorptivity to human body tissues [8], [9]. Therefore, providing a certain level of shielding between the smartphone and the human body meanwhile improving radiation efficiency becomes a solution worthy of investigation.

The concept of metamaterial has been widely applied in antenna design for miniaturization [10], [11], bandwidth [6], [12], [13], [14], gain [15], [16], [17], [18], [19], [20], [21] and radiation efficiency enhancement [22], [23], [24], [25]. For example, a coplanar waveguide (CPW) antenna over a 5×5 metasurface array operating at 2.45 GHz and 5.2 GHz was presented in [26], the gain is 5.17 dB higher than the antenna standalone in two bands, but the bandwidth is narrow (80 MHz). Works in [14] proposed a metasurface that increases

Manuscript received XX, 2024; revised XX; accepted XX. Date of publication XX; date of current version XX. This work was partially supported by the Natural Science Foundation of Shanghai under Grant (24ZR1403100), the Fundamental Research Funds for the Central Universities (2232022D-29), Shanghai Sailing Program (22YF1401000), XJTLU AI University Research Centre, Jiangsu Province Engineering Research Centre of Data Science and Cognitive Computation at XJTLU and SIP AI innovation platform (YZCXPT2022103). *(Corresponding author: Rui Pei)*

M. Zhai and W. Tian are with the College of information science and technology, Donghua University, Shanghai 201620, China, and also with Engineering Research Center of Digitized Textile and Fashion Technology, Ministry of Education, Shanghai, China. (e-mail: mlzhai@dhu.edu.cn)

R. Pei, M. Leach, E. G. Lim, Z. Wang, and J. Wang, are with the School of Advanced Technology, Xi'an Jiaotong Liverpool University, Suzhou 215123, China. (rui.pei@xjtlu.edu.cn)

C. Xu is with vivo mobile Communication Co., Ltd. (email: chenxu.cx@vivo.com)

Q. Hua is with Department of Engineering and Technology, School of Computing and Engineering, University of Huddersfield, HD1 3DH Huddersfield, U.K.

M. O. Akinsolu is with the Faculty of Arts, Science and Technology, Wrexham University, LL11 2AW Wrexham, U.K.

B. Liu is with the James Watt School of Engineering, University of Glasgow, G12 8LU Glasgow, U.K. (e-mail: bo.liu@glasgow.ac.uk)

Y. Huang is with the Department of Electrical Engineering and Electronics, University of Liverpool, Liverpool L69 3BX, U.K.

the antenna gain and also expands the bandwidth, with a bandwidth increase of 17.9 %, but there is no mention of the antenna's effect on the human body. A 4×4 dual-band metasurface that can reduce SAR and increase gain was proposed in [27], and SAR can be reduced by 99%, while [28], [29], [30] proposed and investigated the effect of metasurface bending, which improves human wearable comfort, but the structure is more complicated. There is also little mention of improving antenna radiation efficiency.

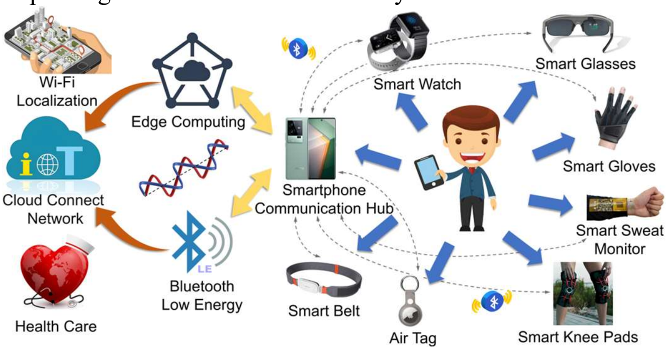

Fig. 1. A wireless communication scenario with human/smartphone as the center for services.

Many works about all-textile reflective metasurface have been used with antenna in on-body scenario [31], [32], [33], [34], [35]. When the antenna is placed very close to the human body, certain distortions in performance would happen. These distortions include frequency shift, gain degradation, and most importantly, a reduction in radiation efficiency. In this study, we propose a metapocket – an all-textile reflective metasurface design operating at the 2.45 GHz band that improves the smartphone antenna gain and radiation efficiency in an on-body scenario. An effective way to accurately measure the on-body radiation efficiency is with a reverberation chamber.

Previous studies have performed such measurements for textile/wearable antennas[36], [37], [38], [39], [40]. However, these studies focused on antennas specifically designed to be attached on the human body. To the authors' best knowledge, there is no study that measures the on-body radiation efficiency improvement for an arbitrary antenna (in this case: a smartphone antenna) close to the human body with a metasurface applied. Moreover, the conductivity of the conductive textile material is crucial as ohmic loss would cause degradation to the radiation efficiency. Fabricating square patch antennas with textile materials of interest and measuring the radiation efficiency in the reverberation chamber can help accurately determine the conductivity of the conductive textile material. There are few prior studies on determining the actual conductivity of textile material at the radio frequency range. The reverberation chamber measurements are crucial in both the fabrication and the performance measurement of the metasurface.

In this paper, the design of metapocket is presented. A parametric study regarding the dimensions of unit cell, the thickness of textile substrate, and the number of unit cells under the condition of a fixed pocket area is investigated. An AI-driven antenna design algorithm is applied to automatically determine the optimized design. The gain and radiation efficiency enhancement effect of the metapocket is simulated with a voxel human model and two types of antennas: frame antenna (FA) from a smartphone (vivo iQOO) and a typical planar inverted-F antenna (PIFA) for comparison. Prior to fabrication, the dielectric constant and the surface conductivity are measured. The all-fabric metapocket is then measured in both an anechoic chamber and a reverberation chamber. Both the simulation and measured results support the effectiveness of the design.

The novelty of this work lies in the following aspects:

(a) First mention of the concept "metapocket", aiming at increasing smartphone antenna radiation performance on human body. This design fits the scenario where smartphone functions as communication and data processing hub for a number of wearable/IoT devices.

(b) This study included a state-of-the-art smartphone antenna design for analysis. The process considered a large metallic backboard behind the smartphone screen and evaluated its impact on body with/without the metapocket.

(c) Considering the special nature of textile material, the thickness and unit cell number are optimized by AI-driven algorithm, which is different from metasurface design fabricated with printed circuit board (PCB) technology.

(d) This study presents two novel applications for reverberation chamber measurement: i) determining the surface conductivity of conductive textile material at radiofrequency band; ii) measuring the radiation efficiency of the smartphone antenna with/without the metapocket on human body.

II. Design and Optimization

A. Overall design logic

With continuous upgrades with computational power network connection, smartphones now act as crucial data transmission/processing and control terminals linked to different wearable devices. However, when smartphones are placed in close proximity to the human body, likely placed in pockets, energy absorption in body tissues and hence significant degradation in radiation efficiency would cause a severe attenuation in the communication channel. In response to these challenges, this paper introduces the concept of the "metapocket", as shown in Fig. 2 (a) which integrates an all-textile reflective metasurface into the pocket, designed to enhance smartphone antenna gain, and radiation efficiency, and reduce SAR. A typical modern smartphone structure is illustrated in Fig. 2 (b). It should be noted that there is a layer of copper cooling sheet placed behind the smartphone's screen. It is already in use on many smartphones mainly for heat dissipation, yet it also serves as a ground plane for smartphone antennas considering its sheer size in the structure. A large metal ground plane can have a significant impact on the radiation pattern of the antenna. Additionally, the orientation (front or back) and random angles at which the smartphone is placed as shown in Fig. 2 (a) in the pocket also can affect antenna performance and should be considered. Aside from these factors, the pocket area is also limited. However, there is a new degree of freedom in the design, the thickness of the substrate, due to the nature of the textile material employed.

Considering the above-mentioned factors, the smartphone including a large metallic ground plane is accurately modeled and simulated. To cope with the arbitrary angle of the smartphone located in the pocket, a cut-corner patch structure with polarization-independent reflective properties is chosen as the design basis of metapocket. In the design process, parameters including the thickness of the substrate and total unit cell number under a fixed pocket area are taken into consideration and imported to an AI-driven antenna design algorithm.

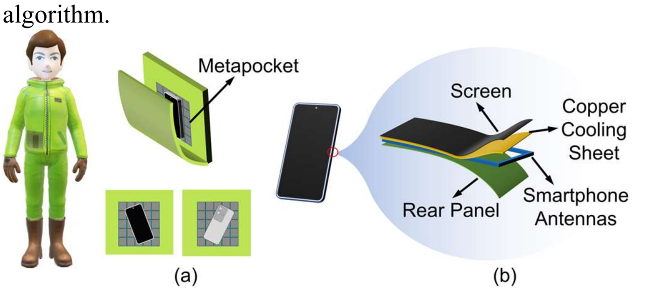

Fig. 2. Overall design logic: (a) design concept of metapocket (b) simplified smartphone structure.

B. Metapocket Design

(I). Basic unit cell Design

The schematic (top and side view) of the metapocket unit cell with polarization insensitivity is shown in Fig. 3 (a). The gray part is the top conductive layer (conductive fibers woven with a plain weave structure, achieving a resistivity of 19.8286 $m\Omega/sq$), the blue part is the felt substrate (wool blend felt with relative permittivity = 1.2 and dielectric tan δ = 0.05). The patches with four corners cut are to achieve polarization-insensitivity for the uncertainty of the smartphone angle in the pocket. The patch length and corner length are described by a and b, respectively; the substrate length and height are depicted by w and t. The value gap denotes the gap between two unit cells as shown in Fig. 3 (b), arranging $n \times n$ metapocket layout in the case of pocket with area dimension $w_{\text{pocket}} \times w_{\text{pocket}}$. The period of metapocket unit cell is w, when w is fixed, the reflection coefficient and reflection phase can be fine-tuned by varying parameters a, b.

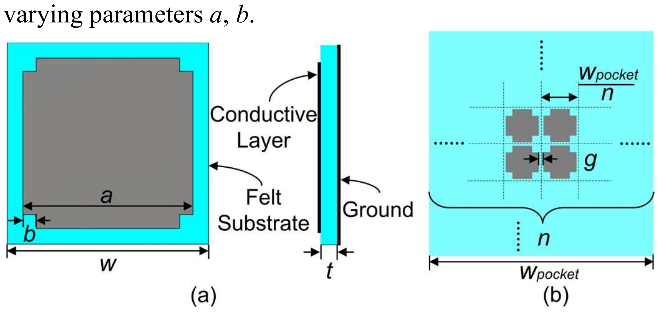

Fig. 3. Metapocket (a) unit cell configuration (b) layout configuration.

The effect of the corner length b and gap g on the reflection phase is shown in Fig. 4 (a). It can be seen that variations in both parameters would cause resonance frequency shift and hence alter the 0-degree reflection frequency. The effect of changing the value gap is much more significant than changing the value b. This becomes a challenge in manufacturing as for full textile structure, fabrication accuracy cannot exceed 1 mm level. Considering the limitation in textile fabrication, the parameter b here serves as a fine tuning parameter for resonance frequency.

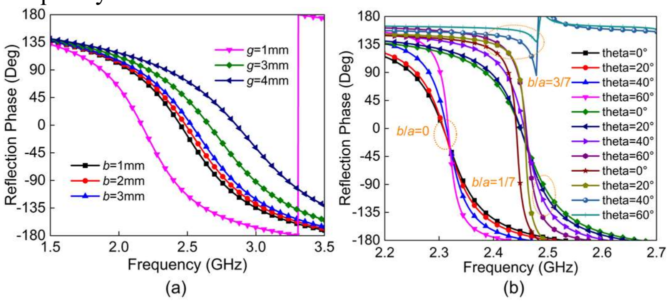

Fig. 4. (a) Simulated reflection performance in varying g and b (b) simulated reflection phase in varying b/a and incidence angle.

Fig. 4 (b) shows the influence of the ratio b/a and incidence angle theta on the reflection phase of metapocket, while keeping g and t constant, with $b/a \in [0, 1/2)$. It can be observed that as b/a increases, the reflection phase bandwidth becomes narrower, and the sensitivity to the incidence angle increases. A larger ratio of b/a, greater than 1/7 would cause the unit cell to resonate similarly to a cross shape rather than a square patch, hence there is a limit for controlling the frequency with the value b.

(II). Parametric study for the Metapocket

Considering the ideal theoretical/simulation case of an infinite number of periodical metapocket unit cells, it can be assumed that an increase in the number of metapocket unit cells and metasurface area leads to better antenna performance. However, in real-life scenarios, the available area of textile behind the smartphone is still limited due to cost and ergonomics concerns. This study focused on determining the optimal selection of metapocket unit cells with a fixed area. Considering the common smartphone/pocket size, the available properties of textile materials, fabrication accuracy, and cost limit, this paper investigates the optimal selection of the number of metapocket unit cells with fixed total area and fixed gap.

The core property to look for is to maintain the resonant frequency f_0 for the metapocket at 2.45 GHz. The preliminary parameters for different unit cell numbers were firstly set with the fixed constraint of an overall size of 180 × 180 mm^2 and a corner ratio b/a =1/7. Then for each case, the self-adaptive Bayesian neural network surrogate model-assisted differential evolution for antenna optimization (SB-SADEA) method [41] is used to search for the optimal parameters. The logic behind the parameters' determination process is summarized in TABLE I. The metapockets' key dimensions during this process are recorded. It is noted that the SADEA series is a well-known effective method for antenna design exploration, and SB-SADEA is the latest version. Particularly, for geometric constraints in the metapocket, the SADEA series has a good ability to handle them. Hence, SB-SADEA is employed. It should be noted that, SB-SADEA is not the exclusive method, and other effective methods, such as [42], can also be used.

TABLE I
PARAMETERS DETERMINATION PROCESS

Objective: Zero-phase-shift at 2.45 GHz
Subject to: nw=180, b/a<1/7, n=3,4,5, …,9
Initialization parameter according to cell number n
Employ the SB-SADEA Algorithm
for *constraints* **do**
  calculate S11 phase at 2.45 GHz.
  if (S11 phase = 0) **then**
    print (‘w, a, t, b’)

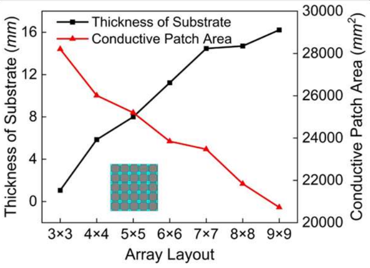

Fig. 5. Relationship between thickness of substrate and conductive patch area.

The relationship between substrate thickness and conductive patch area is visualized in Fig. 5. It reveals that the higher the thickness of the unit cell, the smaller total conductive patch area can be achieved. In the meantime, the reduction of the thickness leads to the reduction of the reflection phase bandwidth of the metapocket structure. The reflection phase bandwidth of metasurfaces with 7 different unit cell numbers, which corresponds to 7 different substrate thicknesses, are shown in Fig. 6. From the figure, it can be seen that the metapocket bandwidth of 7×7, 8×8 and 9×9 setup is close to overlapping, which indicates that the bandwidth enhancement effect is weakened when the unit cell number/thickness reaches a certain level. Overall, a trade-off between the upper patch area, the thickness of the textile substrate and the total number of unit cells can be made to suit textile with different thicknesses, control the amount of conductive fiber used, and maintain a desirable reflection bandwidth. After these considerations, a 5×5 metapocket structure is selected as the desirable structure for the fixed-area pocket scenario. The detailed metapocket parameters are shown in TABLE II with material and fabrication limitations considered.

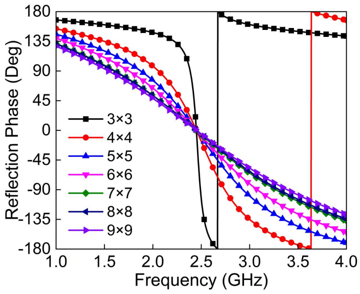

Fig. 6. Reflection phase of different array layouts.

TABLE II
OPTIMIZED METAPOCKET PARAMETERS

Optimized Array Size	$w(mm)$	$a(mm)$	$t(mm)$	$b(mm)$
5×5	36	32	8	2

C. Performance evaluation and principle analysis

Computer Simulation Technology Microwave Studio (CST MWS) is used to perform simulations of the metapocket, the template used is MW&RF&OPTICAL, FSS, Metamaterial-Unit cell, Frequency Domain. The mesh type is Tetrahedral, the total number of grids is 7623, and cells per max box edge of Model and Background is 10 and 1, respectively. The boundary conditions for both X and Y are unit cell, Zmax is open, and Zmin is electric (Et=0) as shown in Fig. 7 (a). The simulation parameters are shown in TABLE II. The reflection coefficient and reflection phase of the proposed design for the normal incidence of wave are shown in Fig. 7 (b). The corresponding reflectivity is larger than 97.78% in the operating frequency band mainly due to the low loss in the substrate material. The metapocket bandwidth ranges from 2.075-2.739 GHz with -90° to 90° criterion to ensure the additive superposition of reflected wave and incident wave.

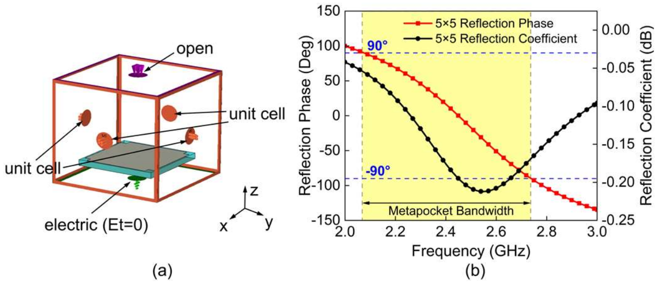

Fig. 7. Metapocket unit cell evaluation (a) boundary conditions setup (b) reflection performance.

Furthermore, since this structure maintains its symmetrical nature, it possesses the property of polarization insensitivity. The reflection coefficient and phase properties with different polarization angles of the incident wave on the metapocket structure are summarized in Fig. 8. It can be seen that the reflection properties remain stable with the polarization angle ranging from 0° to 90°.

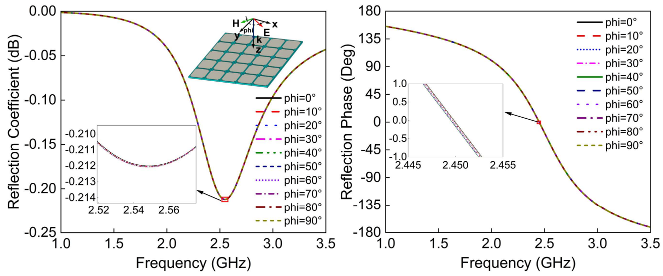

Fig. 8. Polarization independent of proposed metapocket (a) configuration and reflection coefficient (b) reflection phase.

The equivalent circuit model (ECM) of the metapocket in this paper is an R-L-C parallel model, as shown in Fig. 9, where L is the equivalent inductance introduced due to the resonance of the metal patch and the metal ground at the time of the incident electromagnetic wave, C_1 is the equivalent capacitance that exists due to the spacing between neighboring unit cells, R is the equivalent resistance due to the conductive and the dielectric loss of felt, C_2 is the equivalent capacitance due to the capacitive effect between the conductive layer and the ground, while ω is the corresponding frequency.

The surface impedance Z_{HIS} is given by Equation (1), where Z_1 is the input impedance on the conductive layer and Z_2 is the input impedance between the conductive layer and the ground. In this ECM, Equation (2) is satisfied at the resonance point, meanwhile, Z_{HIS} in Equation (1) will exhibit infinite surface impedance, and the surface impedance characteristics of metapocket is shown in Fig. 10 (a). Equation (3) is the reflection phase θ produced by the metapocket, η is the wave impedance in free space. At the resonant frequency of the metapocket, the Z_{HIS} is close to infinity, at which time θ is close to 0 degree and exhibits the characteristics of the metapocket. Fig. 10 (b) shows a comparison of the reflection phase and reflection coefficient of the 5 × 5 metapocket simulation and its ECM, which proves the underlying principle of the unit cell.

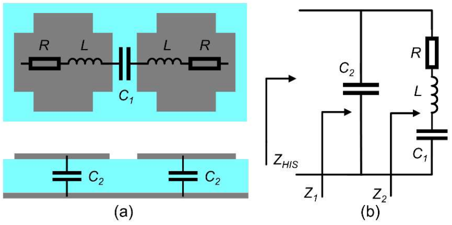

Fig. 9. Equivalent circuit model of design.

$$Z_{HIS} = Z_1 + Z_2 = \frac{1}{\frac{1}{R} + jw\left(C_2 + \frac{C_1}{1-\omega^2 L C_1}\right)} \tag{1}$$

$$\omega_0 = \frac{1}{\sqrt{LC}} \tag{2}$$

$$\theta = \mathrm{Im}\left[\ln\left(\frac{Z_{HIS}-\eta}{Z_{HIS}+\eta}\right)\right] \tag{3}$$

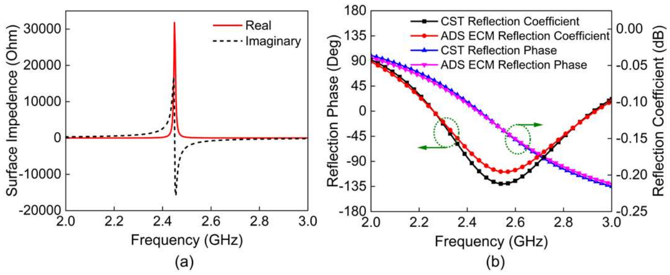

Fig. 10. (a) HIS of design (b) performance comparison of simulation and ECM.

III. Simulation and Analysis

A. Integrated analysis of smartphone-Metapocket-body

(I). Analysis of two typical smartphone antenna structure

Currently, most of the smartphone antennas used are built-in antennas integrated with the circuit board or the metallic frame of the smartphone body. Modern smartphones have dedicated great effort to heat dissipation. Design engineers would include larger copper foil, heat sink, or vapor chamber close to the middle frame of the phone. These designs would function as a large ground plane for antennas integrated nearby and hence have a significant impact on the radiation pattern.

In order to increase the practicality and authenticity, this study bases the design on a smartphone from vivo. This model utilizes laser direct structured (LDS) FA with Fig. 11 (a). The antennas are remodeled in CST for simulation and a 2-by-2 multiple input multiple output (MIMO) setup is used, as shown in Fig. 11 (b). It can also be seen in this figure that the large conductive ground plane is placed parallel to the antenna. In order to further generalize the results for arbitrary antenna setup, a classic PIFA antenna is also modeled and simulated as a comparison. The S-parameters of these two types of antennas are summarized in Fig. 11 (c).

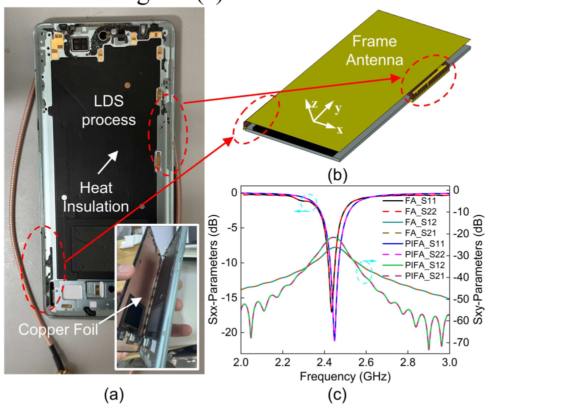

Fig. 11. Frame antenna of smartphone (a) configuration (b) remodeled FA in CST (c) S-parameters of FA and PIFA.

B. Analysis of off-body Gain Enhancement with Metapocket

A complete smartphone model (with PIFA and FA, respectively) is placed on the metapocket for full wave simulation. Fig. 12 (a) illustrates the schematic diagram and S11, the separation distance between the antenna and metapocket is 2 mm (0.016 λ_0) considering the structure of the smartphone. It can be observed that the antenna's matching is maintained relatively well with only a slight frequency shift. The realized gain and radiation efficiency and front-back ratio (FBR) of smartphone antennas with and without metapocket are compared in Fig. 12 (b)-(d).

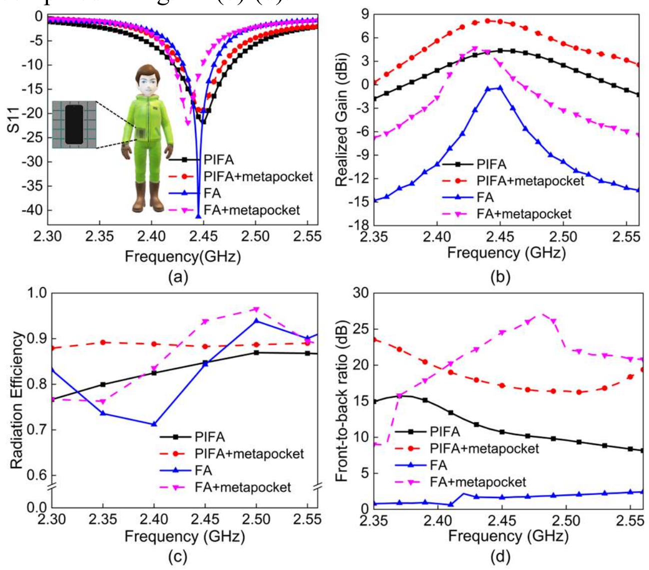

Fig. 12. Reflection performance comparison for off-body scenario (a) schematic diagram and S11 (b) realized gain (c) radiation efficiency (d) FBR.

The results show that the realized gain of both the PIFA and the FA at resonance are improved, proving that a valid additive superposition has been achieved. For the PIFA case, realized gain increases by up to 4.13 dB, FBR by up to 10.01 dB, and radiation efficiency by up to 9.2%. For the FA case, adding metapocket can increase the realized gain by up to 9.96 dB, FBR by up to 25.39 dB, and radiation efficiency by up to 12.4%. The proposed metapocket can achieve gain-enhancement for both smartphone antennas, and reduce the backward radiation.

The difference in performance improvement level is mainly related to the structure of the two antennas. The classic PIFA uses a complete ground plane structure. As a result, the gain and FBR for the PIFA is relatively higher than that for the FA. It is also observed that the antenna with metapocket has a slight frequency deviation, which is mainly due to the introduction of equivalent capacitance after loading the metapocket.

Normalized simulated radiation patterns in the off-body scenario of PIFA and FA with/without metapocket are shown in Fig. 13. The enhancement in gain and FBR can be seen in all four cases. It should be noted that a significant null appears in Fig. 13 (d), this is mainly due to the fact that the antenna in simulation is located on one side of smartphone middle frame.

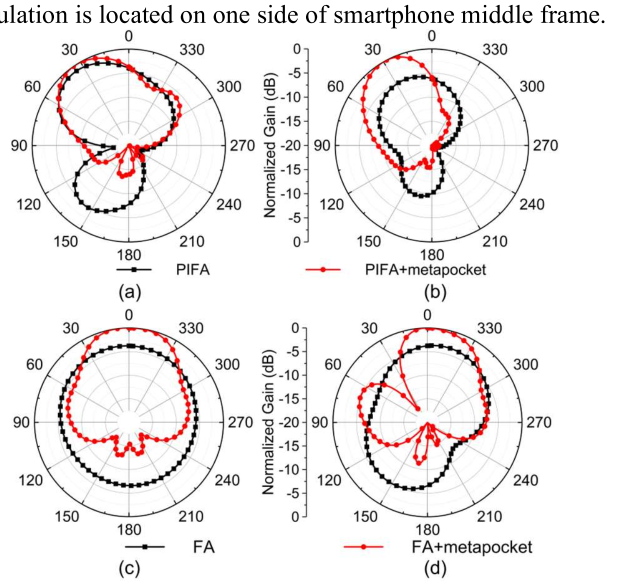

Fig. 13. Off-body normalized simulated radiation patterns of smartphone antenna with/without metapocket (a) xoy-plane of PIFA (b) yoz-plane of PIFA (c) xoy-plane of FA (d) yoz-plane of FA.

C. Analysis of Overall on-body Radiation Improvement

Owing to the fact that the human body absorbs electromagnetic waves, the smartphone antenna performance in the pocket will be affected. Therefore, it is vital to evaluate the on-body effect of metapocket in this scenario. Fig. 14 (a) illustrates the schematic diagram of a smartphone antenna with metapocket on the voxel model Gustav and S11 of on-body effect. The effect of smartphone placement (screen towards outside, denoted as front in the following context; or screen towards inside, denoted as back) is also taken into account. When the smartphone is placed on the human body with the screen facing out, the configuration of copper foil-smartphone antenna-metapocket-human body is formed, smartphone antenna-copper foil-metapocket-human body structure is formed when the smartphone is placed back.

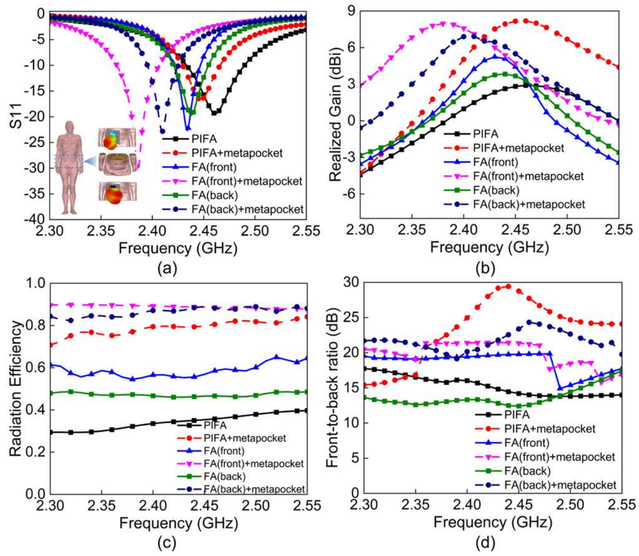

Fig. 14. On-body effect of smartphone antenna with/without metapocket (a) schematic diagram and S11 (b) realized gain (c) radiation efficiency (d) FBR.

The absorption effect of the human body causes a shift in the resonant frequency of the smartphone antenna, as well as a significant reduction in radiation efficiency. Although loading metapocket also results in a certain frequency shift, there is a performance improvement near the resonant frequency. With different smartphone placements, the FA can achieve a realized gain enhancement by 4.32 dB (front), 4.62 dB (back), radiation efficiency is increased by 32.68%, 40.45%, FBR is improved by 2.08 dB, 7.91 dB. The on-body simulation is also performed with the PIFA for comparison, at 2.45 GHz, the realized gain is enhanced by 5.35 dB, radiation efficiency is increased by 44.39%, and the front-to-back ratio is improved by 14.55 dB.

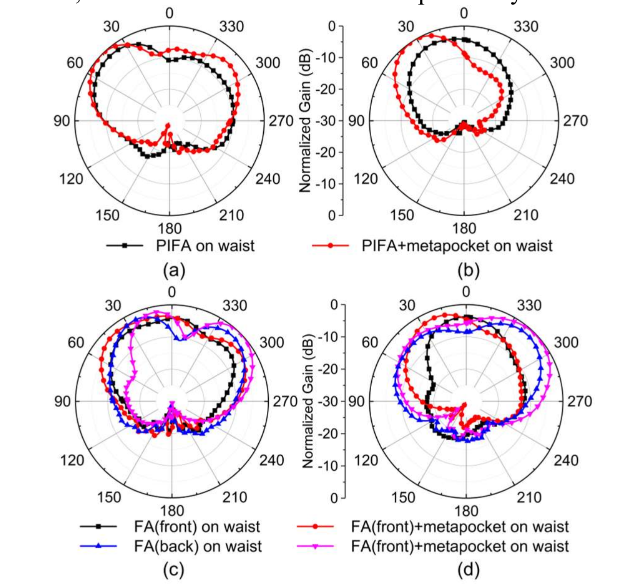

Fig. 15. On-body normalized simulated radiation patterns of smartphone anten na with/without metapocket at 2.45 GHz (a) xoy-plane of PIFA (b) yoz-plane of PIFA (c) xoy-plane of FA (d) yoz-plane of FA.

Fig. 15 shows the normalized radiation patterns of smartphone antennas with/without metapocket at 2.45 GHz. Due to the absorption of electromagnetic waves by the human body, the PIFA and FA exhibit a reduction in gain and radiation efficiency when placed on the body, and some of the backward radiation is also absorbed. In contrast, the smartphone antennas with metapocket at the same position on the human body show a reduction in backward radiation and an increase in gain and radiation efficiency, showing the advantage of metapocket as a reflective surface.

It is also essential to take into account the energy absorption on the human body from smartphone antennas. The SAR value generally describes the electromagnetic power absorbed per unit time per unit mass. This indicator helps to assess the level of different radiation absorption. IEEE C95.1 states that the maximum absorption value for 1 g human tissue should be less than 1.6 W/kg. EN 62209-1 requires a limit value of 2.0 W/kg averaged over 10 g human tissue.

The SAR simulation uses a part of Gustav's waist position. CST MWS is used to calculate the SAR value, the solution is performed using TLM solver after defining the power loss density field monitor at 2.45GHz; the input power is set to 0.5 W, the averaging method is set IEEE/IEC 62704-1. Fig. 16 illustrates the SAR simulation for 10 g tissue of PIFA and FA on the waist with and without metapocket at 2.45 GHz. The SAR values on the waist for 1 g of tissue and 10 g of tissue are shown in TABLE III. All the results with metapocket are less than 1.6 *W/kg*. Moreover, the maximum SAR value of the antenna with the metapocket is significantly lower than those without. The introduction of metapocket with PIFA and FA achieved SAR reduction by 92.94%, 84.82%, 87.25% (1 *g*) and 94.67%, 95.24%, 85.19% (10 *g*), respectively.

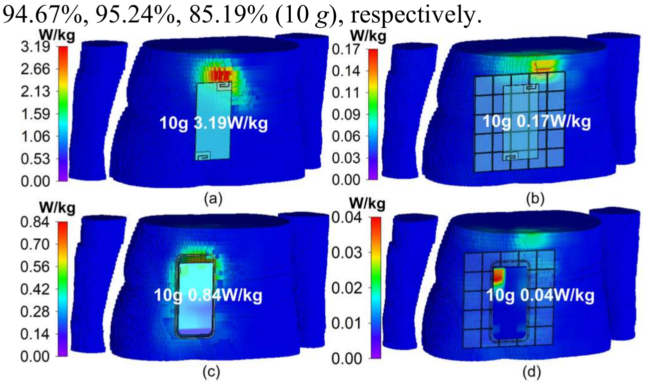

Fig. 16. SAR simulation for 10g tissue on waist of PIFA and FA (a) PIFA (b) PIFA with metapocket (c) FA (d) FA with metapocket.

TABLE III

SAR VALUES ON WAIST IN SIX CASES

SAR (*W/kg*)	FA-front	FA-front+Metapocket	FA-back	FA-back+Metapocket	PIFA	PIFA+Metapocket
1g	1.12	0.17	1.02	0.13	5.22	0.58
10g	0.84	0.04	0.81	0.12	3.19	0.17

IV. FABRICATION AND MEASUREMENT

A. Textile material properties measurement

Conductivity is an important parameter for conductive cloth. A 40x magnified microscopic view of the conductive cloth is depicted in Fig. 17 (a), manifesting its structural uniformity to achieve high and consistent conductivity. A four-probe surface resistivity measurement instrument is used to preliminary measure the surface resistivity, as shown in Fig. 17 (b). By placing four probes equally spaced on the surface of conductive cloth sample, two probes are used to apply current and the other two are used to measure voltage. The resistivity can be calculated by measuring the voltage and current. This measurement can avoid measurement errors due to contact resistance between the probe and the sample with DC voltage. The measured square resistivity of the conductive cloth sample is 19.8286 *Ω/sq*, equivalent to 4.896×10^5 *S/m* with calculation. At higher frequencies, the conductivity value could alter.

The electric conductivity of the conductive cloth sample can also be determined by measuring the radiation efficiency of the antenna in the reverberation chamber. The measurement detail of the reverberation chamber will be covered in IV.*B*.(*II*), this method uses a patch antenna resonating at 2.45 GHz as shown in Fig. 17 (c). Fig. 17 (d) demonstrates the results when conductivity is set to 4.896×10^5 *S/m*, the trends of both curves are basically the same, indicating that the measured conductivity is accurate enough for the intended frequency.

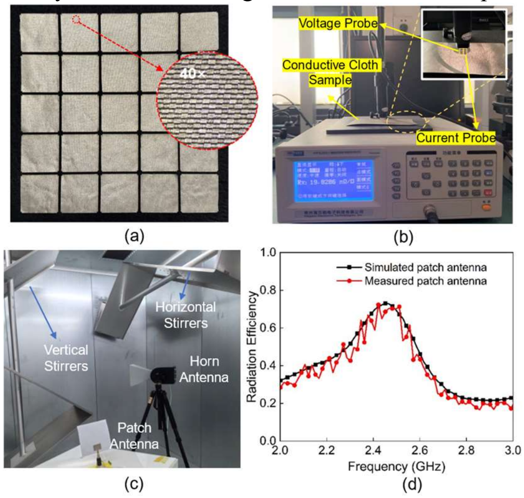

Fig. 17. (a) 40x magnified view of sample (b) Four-point probe resistance measurement configuration for resistivity measurement (c) Kelvin's method for conductivity measurement (d) results of measured and simulated radiation efficiency.

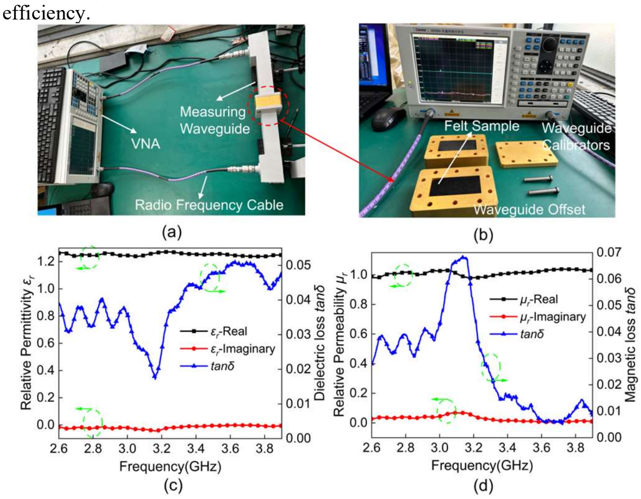

Fig. 18. Electromagnetic performance of felt sample by waveguide transmission line method (a) setup configuration (b) waveguide calibrators (c) electronic properties (d) magnetic properties.

The electromagnetic properties of the substrate material are measured with the test setup shown in Fig. 18 (a). The waveguide transmission line method is used to measure the relative permittivity and dielectric loss of the felt. A WR-284 waveguide is adopted with an operation frequency ranging from 2.6 GHz to 3.95 GHz. The measuring waveguide is calibrated with the waveguide calibration set with a Ceyear vector network analysis (VNA) 3656BA. The measured results of the felt are shown in Fig. 18 (c) and (d). Results show that the measured average relative permittivity of felt sample is 1.25, the average dielectric loss tangent is 0.039, the measured average relative permeability is 1.013, and the average magnetic loss is 0.015.

B. Metapocket Performance Measurement

(I). Gain Measurement in Anechoic Chamber

In this study, a vivo smartphone is used in the tests to verify the effectiveness of smartphone antenna performance enhancement. An anechoic chamber is used to measure the antenna radiation pattern and gain. The schematic diagram of the anechoic chamber test is shown in Fig. 19 (a). When testing in the anechoic chamber, the antenna under test (AUT) is placed at a far-field distance to measure far-field performance, and a set of standard gain horn antennas are used for reference to accurately determine the realized gain. By rotating the antenna or moving the position of the test equipment controlled by a personal computer (PC), performance data of the antenna in different directions can be obtained by VNA. The gain and radiation patterns measurement configuration of the anechoic chamber is shown in Fig. 19 (b).

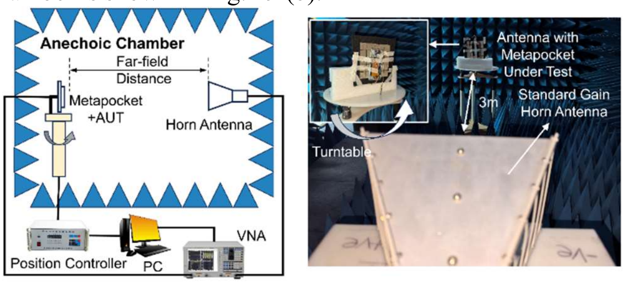

(a) (b)

Fig. 19. Anechoic chamber for far-field measurement (a) schematic diagram (b) measurement configuration.

(II). Radiation Efficiency Measurement in Reverberation Chamber

The reverberation chamber is a special laboratory facility used for electromagnetic compatibility (EMC) testing and antenna measurements. The overview flow chart of measurement is shown in Fig. 20, this method contains one AUT, one reference antenna, a PC and a VNA.

The reverberation chamber setup is illustrated in Fig. 21, the reference antenna refers to an antenna with known radiation efficiency, which is connected to port 1 of the VNA while the AUT is connected to port 2. PC adjusts the rotation angle of the stirrers by controlling the motor controller and collects the S-parameters from the VNA at each stirrer position. The formula used for antenna efficiency measurement is as follows, where <.> represents the averaging of the S-parameter data set obtained with different stirring conditions. The term η_{RAD} is radiation of the AUT, η_{REF} is efficiency of reference antenna.

$$\eta_{RAD} = \left\{ \frac{\left\langle |S_{21AUT}|^2 \right\rangle}{\left\langle |S_{21REF}|^2 \right\rangle} \times \frac{1-|S_{22REF}|^2}{1-|S_{22AUT}|^2} \right\} \times \eta_{REF} \tag{4}$$

It should be noted that for the total radiation efficiency the antenna mismatch loss, denoted as S_{22} in this case, can be measured in an anechoic chamber and the total efficiency can be calculated with the following formula,

$$\eta_{TOTAL} = \eta_{RAD} \times \left(1-(S_{22AUT})^2\right) \tag{5}$$

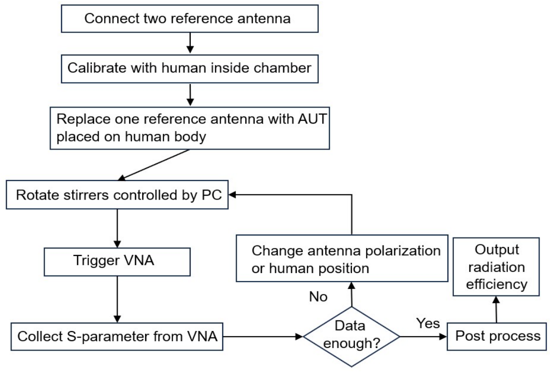

Fig. 20. Overview flow chart for measuring radiation efficiency in reverberati on chamber.

The measurement of smartphone antenna's efficiency generally follows the principle shown with Equations (4) and (5). The main difference is that the human body dominates the losses in the chamber with its presence. The calibration of the chamber needs to be performed with the human body in the chamber as it has a severe loading effect on the chamber. The calibration is performed with two identical reference horn antennas and with the human body (including the same clothing and pocket contents) in the chamber. The S-parameter datasets with the two types of stirring are documented as the reference value. The detailed measurement process is as follows,

i) Calibrate the VNA and set up the reference horn antennas in one position and perform S-parameter measurements with a stepwise changed stirrer position (180 data sets with a 2° step size for both horizontal and vertical stirrer rotations).

ii) Changing the polarization of both antennas and repeating step 1 again (360 data sets acquired at this stage).

iii) Changing the AUT location and performing the previous two steps again. Four different positions are used in this case considering both the test subject's tolerance and the accuracy of the measurement.

iv) The S-parameter measured with two horns are the S_{21REF} and S_{22REF} values. One of the horns is then changed to the smartphone antenna attached to the test subject and the same process is repeated one more time, obtaining S_{21AUT} and S_{22AUT}.

It should be noted that enough data points must be selected to ensure sufficient modes in the chamber. In the measurements in this study, a slightly different setting is used considering the different frequency range, equipment set up and the test subject's tolerance. The stirring sequence for the off-body measurement in this study includes mechanical stirring (2 degrees, 180 measurements), polarization stirring (two orthogonal linear polarizations) and position stirring (4 receiver positions). A total of 1440 datasets are documented for each run to calculate the efficiency in this study. With the calibration run (two horns) and the measurement run (AUT off-body and one horn), 2880 datasets are used for the whole calculation process.

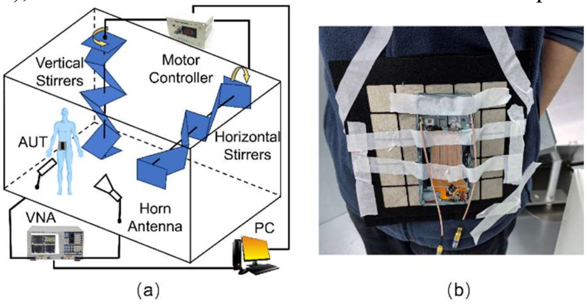

Fig. 21. Reverberation chamber for radiation efficiency measurement (a) sche matic diagram (b) metapocket on the human body.

C. Measurement Results and Analysis

Fig. 22 illustrates the normalized measured radiation patterns of smartphone antenna with/without metapocket in the xoz-plane and yoz-plane at 2.4 GHz. A significant reduction in the backward radiation can be observed. The radiation pattern is more concentrated around 30°, which is related to the position of the smartphone antenna on the metallic frame, and the realized gain has increased by approximately 3.17 dB.

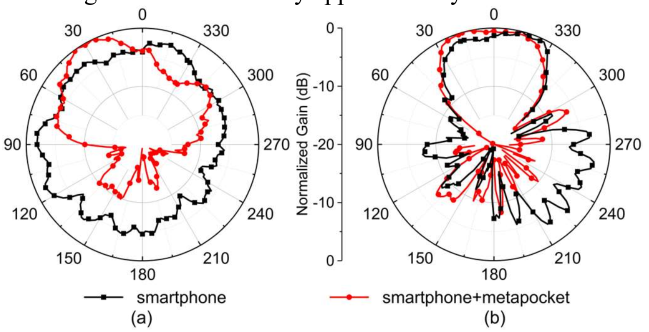

Fig. 22. Normalized measured radiation patterns of smartphone at 2.45 GHz (a) xoz-plane (b) yoz-plane.

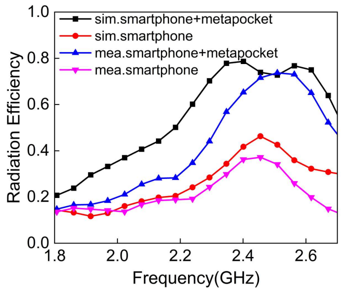

Fig. 23. Measured and simulated radiation efficiency of smartphone antenna with/without metapocket in an on-body scenario.

As shown in Fig. 23, a comparative analysis is presented of simulated and measured radiation efficiencies in an on-body scenario. Results reveal that the simulated and measured data exhibit a similar trend, the measured radiation efficiency has increased by 34.37% at 2.45 GHz and by up to 47.13% at 2.56 GHz. Notably, the introduction of the metapocket has led to two slightly separated peaks, which are likely a consequence of the alight frequency shift induced by the metapocket. The measured results support that the introduction of the metapocket improves the radiation efficiency and enhances the ability of the smartphone antenna to send and receive signals, which is an improvement of significant value to on-body wireless communication.

The gain and radiation efficiency of smartphone antennas achieved in this study are compared with other reported state-of-the-art works, as listed in TABLE IV. Compared with metasurface in [11], [18], [19], [20], [23], the proposed design utilizes a more flexible material, which is beneficial for wearable applications. Compared with metasurfaces in [11], [23], [24], [28], this work has a smaller distance between the antenna and the metapocket, allowing for an ergonomic and low-profile design. Compared with metasurfaces in [11], [19], [21], [24], the proposed design has higher gain enhancement. Compared with metasurfaces in [23], [24], [28], the proposed design achieves higher radiation efficiency enhancement. Meanwhile, [23], [25], [28] achieved higher gain enhancement compared with this work, mainly due to the benefit of designing an antenna with integrated metasurface. It is noted that the work in [25] has both higher gain and radiation efficiency than this work, but has higher separation distance. For the proposed work, the band of 2.075-2.739 GHz can be applied in Wi-Fi, Bluetooth, 5G n41 bands for 5G communication, IoT, IoV applications.

V. Conclusion

A polarization-independent all-textile metapocket for enhancing gain and radiation efficiency and reducing SAR of smartphone antenna applications has been presented in this paper. After a preliminary investigation into the impact of unit cell numbers on reflectivity performance, the SB-SADEA algorithm is used to generate a number of designs and search for the best parameter set, resulting in the proposed structure with a bandwidth of 2.075-2.739 GHz and reflectivity greater than 97.78%. The symmetric nature of the structure confers polarization insensitivity, and the reflection mechanism is studied by analyzing the equivalent circuit model. Two types of smartphone antennas, PIFA and FA, are used to explore the performance enhancement of metapocket. Simulation results show that the maximum realized gain could be increased by 4.131 dB, and the radiation efficiency improved by 13%. Considering wearable scenarios, simulations on-body are also conducted, and the results indicate that the structure could achieve over 95% SAR reduction. Finally, the smartphone antenna from vivo is measured in both the reverberation chamber and the anechoic chamber. The antenna gain could be improved by 3.17 dB, and on-body radiation efficiency could be increased by a maximum of 34.37%. Finally, enhancing smartphone antenna performance positions the proposed metapocket as an excellent candidate for 5G communication, IoT, and wearable applications.

Acknowledgment

The authors would like to thank CST AG for providing the CST Studio Suite Electromagnetic Simulation Software package under the China Key University Promotion Program.

TABLE IV
COMPARISON OF PREVIOUS RELATED WORKS

Ref.	Frequency (GHz)	Type of substrate	Antenna Type	Separation distance between antenna and metasurface	Gain enhancement (dB)	Radiation efficiency enhancement
[11](2023)	4.04	FR4 (ε_r=4.4, tanδ=0.02)	CPW Antenna	25mm	2.5	N/A
[18](2023)	2.40	PEC	CPW Antenna	1mm	3.7	N/A
[19](2012)	2.45	FR4 (ε_r=4.4, tanδ=0.02)	Patch Antenna	N/A	0.8	N/A
[20](2020)	2.4	Rogers RT/duroid 5880(ε_r=2.2, tanδ=0.0009)	Monopole Antenna	15mm	6	N/A
[21](2016)	2.45	Latex (ε_r=3.31, tanδ=0.028)	Yagi Antenna	5.5mm	3.1	N/A
[23](2019)	3-11	RT6010 (ε_r=10.2, tanδ=0.0023)	UWB Antenna	3mm /5mm	4	2%
[24](2018)	2.45	Felt (ε_r=1.2, tanδ=0.02)	Slot Antenna	6mm	2.74	23.6%
[25](2021)	2.45	Felt (ε_r=1.2, tanδ=0.044)	CRLH Antenna	3mm	5.29	72.4%
[28](2023)	1.96-2.81	Felt (ε_r=1.3, tanδ=0.044)	Monopole Antenna	7mm	3.93	9.53%
This work	**2.45**	**Felt (ε_r=1.2, tanδ=0.05)**	**PIFA FA**	**2mm**	**3.17**	**34.37%**

REFERENCES

[1] G. Hong and D. Shin, "Virtual Connection: Selective Connection System for Energy-Efficient Wearable Consumer Electronics," *IEEE Transactions on Consumer Electronics,* vol. 66, no. 4, pp. 299-307, 2020.

[2] A. Nag, S. C. Mukhopadhyay, and J. Kosel, "Wearable Flexible Sensors: A Review," *IEEE Sensors Journal,* vol. 17, no. 13, pp. 3949-3960, 2017.

[3] A. M. Joshi, P. Jain, S. P. Mohanty, and N. Agrawal, "iGLU 2.0: A New Wearable for Accurate Non-Invasive Continuous Serum Glucose Measurement in IoMT Framework," *IEEE Transactions on Consumer Electronics,* vol. 66, no. 4, pp. 327-335, 2020.

[4] S. C. Sethuraman, P. Kompally, S. P. Mohanty, and U. Choppali, "MyWear: A Novel Smart Garment for Automatic Continuous Vital Monitoring," *IEEE Transactions on Consumer Electronics,* vol. 67, no. 3, pp. 214-222, 2021.

[5] P. F. Hu and K. W. Leung, "Polarization Diversity Glass Antenna for Consumer WiFi Routers," *IEEE Transactions on Consumer Electronics,* vol. 70, no. 1, pp. 350-357, 2024.

[6] J. H. Lee and J. G. Yook, "Improvement of radiation performance of mobile phone antenna using parasitic element," *IEEE Transactions on Consumer Electronics,* vol. 56, no. 4, pp. 2411-2415, 2010.

[7] M. Y. Liang *et al.*, "High Head–Hand Efficiency and Low-SAR Mobile Phone Antenna Design Based on Unidirectional and Uniform Current Distribution," *IEEE Transactions on Antennas and Propagation,* vol. 72, no. 7, pp. 5560-5568, 2024.

[8] P. L. Carro, J. d. Mingo, P. Garcia-Dúcar, and C. Sánchez, "Performance degradation due to antenna impedance variability in DVB-H consumer devices," *IEEE Transactions on Consumer Electronics,* vol. 56, no. 2, pp. 1153-1159, 2010.

[9] C. Ahn, B. Ahn, S. Kim, and J. Choi, "Experimental outage capacity analysis for off-body wireless body area network channel with transmit diversity," *IEEE Transactions on Consumer Electronics,* vol. 58, no. 2, pp. 274-277, 2012.

[10] L. Murugasamy and R. Sivasamy, "A Single Layer Interdigitated Loop Elements-Based Miniaturized Frequency Selective Surface for WLAN Shielding," *IEEE Transactions on Consumer Electronics,* vol. 70, no. 1, pp. 617-626, 2024.

[11] W.-J. Wu and G. Wang, "A modified AMC-based antenna sensor for contactless measurement of complex permittivity," *Measurement,* vol. 206, p. 112261, 2023/01/01/ 2023.

[12] S. H. Ates, N. Akcam, and T. Okan, "Bandwidth and Gain Enhancement using FSS on CPW-fed Rectangular Patch Antenna for 5G mm-Wave Applications," in *2022 International Congress on Human-Computer Interaction, Optimization and Robotic Applications (HORA)*, 2022, pp. 1-4.

[13] S. Douhi, A. Eddiai, M. Idiri, O. Cherkaoui, and M. h. Mazroui, "Investigation of SAR reduction and gain enhancement using an all-textile antenna with metamaterial structure for wireless body area network

applications," *Materials Today: Proceedings,* 2023/12/25/ 2023.

[14] J. D. Ntawangaheza, L. Sun, and G. Rushingabigwi, "Patch Antenna Bandwidth and Aperture Efficiency Enhancement Using Shorted Microstrip Loop and AMC," in *2019 IEEE 2nd International Conference on Electronic Information and Communication Technology (ICEICT)*, 2019, pp. 792-795.

[15] Y. Yu, Z. Akhter, and A. Shamim, "Improving the Performance of Antenna-on-Chip by Effectively Illuminating the Artificial Magnetic Conductors Through Coupling Enhancement Structures," *IEEE Transactions on Antennas and Propagation,* vol. 71, no. 5, pp. 4492-4497, 2023.

[16] Y. Yu, Z. Akhter, and A. Shamim, "Ultra-Thin Artificial Magnetic Conductor for Gain Enhancement of Antenna-on-Chip," *IEEE Transactions on Antennas and Propagation,* vol. 70, no. 6, pp. 4319-4330, 2022.

[17] H. Malekpoor, "AMC-Loaded Low-Profile Broadband Printed 2×2 Array With Gain and Isolation Enhancement Using Equivalent Circuit Model for Wireless Systems," *IEEE Access,* vol. 11, pp. 22007-22017, 2023.

[18] B. Babu, R. Dewan, N. A. Samsuri, and D. Paramasivam, "Reduced Size Modified Square-Shaped AMC for Antenna Gain Enhancement," in *2023 IEEE International Symposium On Antennas And Propagation (ISAP)*, 2023, pp. 1-2.

[19] M. SalarRahimi, J. Rashed-Mohassel, and M. Edalatipour, "Radiation Properties Enhancement of a GSM/WLAN Microstrip Antenna Using a Dual Band Circularly Symmetric EBG Substrate," *IEEE Transactions on Antennas and Propagation,* vol. 60, no. 11, pp. 5491-5494, 2012.

[20] J. Liu, J. Y. Li, J. J. Yang, Y. X. Qi, and R. Xu, "AMC-Loaded Low-Profile Circularly Polarized Reconfigurable Antenna Array," *IEEE Antennas and Wireless Propagation Letters,* vol. 19, no. 7, pp. 1276-1280, 2020.

[21] K. Agarwal, Y. X. Guo, and B. Salam, "Wearable AMC Backed Near-Endfire Antenna for On-Body Communications on Latex Substrate," *IEEE Transactions on Components, Packaging and Manufacturing Technology,* vol. 6, no. 3, pp. 346-358, 2016.

[22] S. Yang *et al.*, "Compact Tetracyclic Nested AMC-Backed Multiband Antenna With High OoB Rejection and Enhanced Gain Radiation for IIoV-Based Sensing and Communication," *IEEE Internet of Things Journal,* vol. 11, no. 2, pp. 2819-2829, 2024.

[23] Y. Yuan, X. Xi, and Y. Zhao, "Compact UWB FSS reflector for antenna gain enhancement," *IET Microwaves, Antennas & Propagation,* vol. 13, no. 10, pp. 1749-1755, 2019/08/01 2019.

[24] G. P. Gao, B. Hu, S. F. Wang, and C. Yang, "Wearable Circular Ring Slot Antenna With EBG Structure for Wireless Body Area Network," *IEEE Antennas and Wireless Propagation Letters,* vol. 17, no. 3, pp. 434-437, 2018.

[25] M. E. Atrash, M. A. Abdalla, and H. M. Elhennawy, "A Compact Highly Efficient Π-Section CRLH Antenna Loaded With Textile AMC for Wireless Body Area Network Applications," *IEEE Transactions on Antennas and Propagation,* vol. 69, no. 2, pp. 648-657, 2021.

[26] M. Faiza, A. Azrar, M. Dehmas, and K. Djafer, "Gain Enhancement of Monopole Antenna using AMC Surface," *Advanced Electromagnetics,* vol. 7, pp. 69-74, 08/16 2018.

[27] M. E. Atrash, M. A. Abdalla, and H. M. Elhennawy, "A Wearable Dual-Band Low Profile High Gain Low SAR Antenna AMC-Backed for WBAN Applications," *IEEE Transactions on Antennas and Propagation,* vol. 67, no. 10, pp. 6378-6388, 2019.

[28] U. Ali, S. Ullah, A. Basir, B. Kamal, L. Matekovits, and H. Yoo, "Design and SAR Analysis of AMC-Based Fabric Antenna for Body-Centric Communication," *IEEE Access,* vol. 11, pp. 73894-73911, 2023.

[29] R. Pei *et al.*, "Wearable EBG-Backed Belt Antenna for Smart On-Body Applications," *IEEE Transactions on Industrial Informatics,* vol. 16, no. 11, pp. 7177-7189, 2020.

[30] Y. B. Chaouche, M. Nedil, I. B. Mabrouk, and O. M. Ramahi, "A Wearable Circularly Polarized Antenna Backed by AMC Reflector for WBAN Communications," *IEEE Access,* vol. 10, pp. 12838-12852, 2022.

[31] A. B. Dey, S. Kumar, W. Arif, and J. Anguera, "Elastomeric Textile Substrates to Design a Compact, Low-Profile AMC-Based Antenna for Medical and IoT Applications," *IEEE Internet of Things Journal,* vol. 10, no. 6, pp. 4952-4969, 2023.

[32] H. Yang, X. Liu, and Y. Fan, "Design of Broadband Circularly Polarized All-Textile Antenna and Its Conformal Array for Wearable Devices," *IEEE Transactions on Antennas and Propagation,* vol. 70, no. 1, pp. 209-220, 2022.

[33] G. P. Gao, C. Yang, B. Hu, R. F. Zhang, and S. F. Wang, "A Wearable PIFA With an All-Textile Metasurface for 5 GHz WBAN Applications," *IEEE Antennas and Wireless Propagation Letters,* vol. 18, no. 2, pp. 288-292, 2019.

[34] K. Zhang, P. J. Soh, and S. Yan, "Design of a Compact Dual-Band Textile Antenna Based on Metasurface," *IEEE Transactions on Biomedical Circuits and Systems,* vol. 16, no. 2, pp. 211-221, 2022.

[35] A. Alemaryeen and S. Noghanian, "On-Body Low-Profile Textile Antenna With Artificial Magnetic Conductor," *IEEE Transactions on Antennas and Propagation,* vol. 67, no. 6, pp. 3649-3656, 2019.

[36] S. J. Boyes, P. J. Soh, Y. Huang, G. A. E. Vandenbosch, and N. Khiabani, "Measurement and Performance of Textile Antenna Efficiency on a Human Body in a Reverberation Chamber," *IEEE Transactions on Antennas and Propagation,* vol. 61, no. 2, pp. 871-881, 2013.

[37] H. Gao, X. Chen, Y. Liu, and G. F. Pedersen, "Antenna Performance Over-the-Air Testing of 5G Commercial Smartphones," *IEEE Transactions on Instrumentation and Measurement,* vol. 73, pp. 1-8, 2024.

[38] I. Duhaini, "The effects of electromagnetic fields on human health," *Physica Medica,* vol. 32, p. 213, 2016/09/01/ 2016.

[39] F. Peng, X. Liu, J. Zheng, R. Chen, S. Zhu, and X. Chen, "An Effective Method for Antenna Radiation Pattern Reconstruction Based on Phaseless Measurement in a

Reverberation Chamber," *IEEE Transactions on Antennas and Propagation,* vol. 71, no. 6, pp. 4747-4758, 2023.

[40] W. Qi *et al.*, "A Fast Time-Domain Method of Antenna Efficiency Measurement in a Reverberation Chamber," *IEEE Antennas and Wireless Propagation Letters,* vol. 22, no. 7, pp. 1682-1685, 2023.

[41] Y. Liu *et al.*, "An Efficient Method for Antenna Design Based on a Self-Adaptive Bayesian Neural Network-Assisted Global Optimization Technique," *IEEE Transactions on Antennas and Propagation,* vol. 70, no. 12, pp. 11375-11388, 2022.

[42] A. Papathanasopoulos, P. A. Apostolopoulos, and Y. Rahmat-Samii, "Optimization Assisted by Neural Network-Based Machine Learning in Electromagnetic Applications," *IEEE Transactions on Antennas and Propagation,* vol. 72, no. 1, pp. 160-173, 2024.